

An extended size-luminosity relation for the reverberation-mapped AGNs: the role of the accretion rate

Li-Ming Yu¹, Bi-Xuan Zhao¹, Wei-Hao Bian¹ [★], Chan Wang¹, Xue Ge¹

¹*School of Physics and Technology, Nanjing Normal University, Nanjing 210046, China*

8 April 2024

ABSTRACT

For a compiled sample of 120 reverberation-mapped AGNs, the bivariate correlations of the broad-line regions (BLRs) size (R_{BLR}) with the continuum luminosity at 5100 Å (L_{5100}) and the dimensionless accretion rates (\dot{M}) are investigated. Using our recently calibrated virial factor f , and the velocity tracer from the H β Full-width at half-maximum (FWHM(H β)) or the line dispersion ($\sigma_{\text{H}\beta}$) measured in the mean spectra, three kinds of SMBH masses and \dot{M} are calculated. An extended $R_{\text{BLR}}(\text{H}\beta) - L_{5100}$ relation including \dot{M} is found to be stronger than the canonical $R_{\text{BLR}}(\text{H}\beta) - L_{5100}$ relation, showing smaller scatters. The observational parameters, R_{Fe} (the ratio of optical Fe II to H β line flux) and the line profile parameter $D_{\text{H}\beta}$ ($D_{\text{H}\beta} = \text{FWHM}(\text{H}\beta)/\sigma_{\text{H}\beta}$), have relations with three kinds of \dot{M} . Using R_{Fe} and $D_{\text{H}\beta}$ to substitute \dot{M} , extended empirical $R_{\text{BLR}}(\text{H}\beta) - L_{5100}$ relations are presented. R_{Fe} is a better “fix” for the $R_{\text{BLR}}(\text{H}\beta) - L_{5100}$ offset than the H β shape $D_{\text{H}\beta}$. The extended empirical $R_{\text{BLR}}(\text{H}\beta) - L_{5100}$ relation including R_{Fe} can be used to calculate R_{BLR} , and thus the single-epoch SMBH mass M_{BH} . Our measured accretion rate dependence is not consistent with the simple model of the accretion disk instability leading the BLRs formation. The BLR may instead form from the inner edge of the torus, or from some other means in which BLR size is positively correlated with accretion rate and the SMBH mass.

Key words: galaxies: active galaxies: nuclei galaxies: Seyfert quasars: emission lines quasars: general

1 INTRODUCTION

There is good observational and theoretical evidence that super-massive black holes (SMBHs) exist in nearly every galaxy in universe. Understanding the properties of these SMBHs will clarify their roles in galaxy formation and evolution across the cosmology history (e.g. Kormendy & Ho 2013). There are mainly two parameters for a SMBH, i.e., mass (M_{BH}) and spin, which need to be determined. For a few very nearby (< 100 Mpc) quiescent galaxies, including our Galaxy, SMBH masses can be measured through the stellar or gaseous dynamics method (e.g. Tremaine et al. 2002; McConnell et al. 2011). It has been found that nearby quiescent galaxies follow a tight correlation between the central SMBH mass and the bulge or spheroid stellar velocity dispersion (σ_*), which is called $M_{\text{BH}} - \sigma_*$ relation (e.g. Kormendy & Ho 2013). AGNs can be classified into type 1 or type 2 AGNs, depending on whether the broad-line regions (BLRs) can be viewed directly. For type 1 AGN, the BLR can be used as a probe of the gravitational potential of the SMBHs. The SMBH mass can be weighed through the BLRs clouds for type I AGNs across cosmos time. The SMBH masses

in type I AGNs can be calculated as follows (e.g. Kaspi et al. 2000; Bian & Zhao 2002; Peterson et al. 2004; Collin et al. 2006; Du et al. 2016a; Yu et al. 2019):

$$M_{\text{BH}} = f_{\text{BLR}} \frac{R_{\text{BLR}} (\Delta V)^2}{G}. \quad (1)$$

where G is the gravitational constant. R_{BLR} is the distance from black hole to the BLRs, and can be estimated from the reverberation mapping (RM) method (e.g. Blandford & McKee 1982; Peterson 1993). ΔV is the velocity of the BLRs clouds, and usually traced by the Full-width at half-maximum (FWHM) or the line dispersion ($\sigma_{\text{H}\beta}$) of the broad H β emission line. f_{BLR} is a virial factor to characterize the kinematics, geometry, inclination of the BLRs clouds. Using the $M_{\text{BH}} - \sigma_*$ relation, we recently did the calibration of f_{BLR} and found $f_{\text{BLR}} \propto \text{FWHM}^{-1.11}$ when FWHM(H β) is used as the tracer of ΔV in Equation 1 (Mejia-Restrepo et al. 2018; Yu et al. 2019). It is consistent with the results by the BLRs dynamical model to fit simultaneously the AGNs continuum/H β light curves and H β line profiles (e.g. Li et al. 2018; Pancoast et al. 2018; Williams et al. 2018).

To weigh SMBH masses in AGNs, R_{BLR} is a key paramete-

[★] E-mail: whbian@njnu.edu.cn

ter in Equation 1. Considering the photonization model of the BLRs in AGNs, the variance of the central ionization luminosity leads to the variability of the emission line luminosity in the BLRs, but with a time lag τ (i.e. the RM technique). $R_{\text{BLR}} = c\tau$ can be estimated, and the lag time τ was successfully measured by the RM method for nearly 120 AGNs (e.g. Peterson et al. 2004; Grier et al. 2017; Fausnaugh et al. 2017; Du et al. 2018). An empirical $R_{\text{BLR}}(\text{H}\beta) - L_{5100}$ relation for the $\text{H}\beta$ broad line is derived based on the RM AGNs and is also suggested in a single AGN. (Kaspi et al. 2000, 2005; Bentz et al. 2013; Kilerci Eser et al. 2015; Du et al. 2018):

$$R_{\text{BLR}}(\text{H}\beta) = \alpha l_{44}^{\beta} \text{ ltd.} \quad (2)$$

where $l_{44} = L_{5100}/10^{44} \text{ erg s}^{-1}$ is the 5100 Å luminosity in units of $10^{44} \text{ erg s}^{-1}$ and $R_{\text{BLR}}(\text{H}\beta) = c\tau$ is the emissivity-weighted radius of the BLRs (Kaspi et al. 2000; Bentz et al. 2013). This empirical $R_{\text{BLR}}(\text{H}\beta) - L_{5100}$ relation is widely calibrated and used to calculate the single-epoch M_{BH} for AGNs showing broad emission-lines from a flux-calibrated spectrum (e.g. Bian & Zhao 2004; Vestergaard & Peterson 2006; Bian et al. 2008; Shen et al. 2011; Ge et al. 2016). Subtracting the starlight contribution at 5100 Å by decomposing the two-dimensional surface brightness of the host galaxies of RM AGNs imaged by HST, Bentz et al. (2013) found that $\beta = 0.533 \pm 0.03$ instead of previous value of 0.70 ± 0.03 by Kaspi et al. (2000).

For a large RM campaign of super-Eddington accreting massive black holes (SEAMBHs) in AGNs (Wang et al. 2013), it was found that the $\text{H}\beta$ time lags of the SEAMBHs are shorter than the values predicted by the canonical $R_{\text{BLR}}(\text{H}\beta) - L_{5100}$ relation of sub-Eddington AGNs, by factors of $\sim 2 - 6$, and the $\text{H}\beta$ size for super-Eddington AGNs ($\dot{\mathcal{M}} \geq 3$) has a dependence on the dimensionless accretion rate $\dot{\mathcal{M}}$ (e.g. Du et al. 2018; Martínez-Aldama et al. 2019). For a high- z sample of 44 RM AGNs ($z \sim 0.1 - 1.0$) from the Sloan Digital Sky Survey (SDSS) RM Project, Grier et al. (2017) measured $\text{H}\beta/\text{H}\alpha$ lags and also found shorter lags for a number of AGNs. The shorter lag is possibly due to the self-shadowing effect in super-Eddington AGNs, the retrograde accretion onto the SMBH in low-accretion rate AGNs (Wang et al. 2014a,b; Du et al. 2018). Recently, it was suggested that the relation between L_{5100} and the ionizing flux L_{ion} is non-linear and depends on the Spectral Energy Distribution (SED) of the source, which would lead to a shorter time lag (Czerny et al. 2019). Considering that the gravitational instability of standard thin accretion disks leads to the BLRs, it was suggested that the BLRs sizes also have a relation with the mass accretion rate (\dot{M}) in addition to the continuum luminosity at 5100 Å, $R_{\text{BLR}} \propto L_{5100}^{0.5} \dot{M}^{-37/45}$ (Bian & Zhao 2002). Therefore, from both sides of RM observation or the BLRs theory, it needs to revise the empirical $R_{\text{BLR}}(\text{H}\beta) - L_{5100}$ relation to consider the effect of the SMBH accretion rate.

The accretion rate can be derived from the disk model of Shakura & Sunyaev (1973), which has been extensively applied to fit the spectra of AGNs (e.g. Davis & Laor 2011; Wang et al. 2014a). Considering that the effective temperature distribution is given by $T_{\text{eff}} \propto R^{-3/4}$ and the effect of the inner boundary can be neglected because the region emitting optical radiation is far from the boundary, the dimensionless accretion rate $\dot{\mathcal{M}}$ is

$$\dot{\mathcal{M}} \equiv \dot{M}/\dot{M}_{\text{Edd}} = 20.1 \left(\frac{l_{44}}{\cos i} \right)^{3/2} m_7^{-2}. \quad (3)$$

where $l_{44} = L_{5100}/10^{44} \text{ erg s}^{-1}$ is the 5100 Å luminosity in units of $10^{44} \text{ erg s}^{-1}$, the Eddington accretion rate is $\dot{M}_{\text{Edd}} \equiv L_{\text{Edd}}/c^2$,

the Eddington luminosity is $L_{\text{Edd}} = 1.5 \times 10^{38} (M_{\text{BH}}/M_{\odot})$, i is the accretion disk inclination relative to the observer, the SMBH mass $m_7 = M_{\text{BH}}/10^7 M_{\odot}$. An average value of $\cos i = 0.75$ is adopted (e.g. Du et al. 2018). The Eddington ratio $L_{\text{Bol}}/L_{\text{Edd}}$ is an important parameter describing the SMBH accretion process, where L_{Bol} is the bolometric luminosity. $L_{\text{Bol}} = k_{5100} \times L_{5100}$, and $k_{5100} = 9$. The bolometric correction coefficient k_{5100} was also suggested to have a dependence on the luminosity or the Eddington ratio (e.g. Marconi et al. 2004; Jin et al. 2012; Wang et al. 2019). For the mass accretion rate \dot{M} , $L_{\text{Bol}} = \eta \dot{M} c^2$, then $L_{\text{Bol}}/L_{\text{Edd}} = \eta \dot{\mathcal{M}}$, where η is the radiative efficiency. If $\eta = 0.1$, then $\dot{\mathcal{M}} = 10 \times L_{\text{Bol}}/L_{\text{Edd}}$. For SEAMBHs, smaller η leads to larger $\dot{\mathcal{M}}$ (e.g. Du et al. 2018).

It was suggested that dimensionless observational parameter R_{Fe} or $D_{\text{H}\beta}$ from the optical spectrum of AGNs can be used to determine the Eddington ratio $\dot{\mathcal{M}}$, where the shape of the $\text{H}\beta$ broad-line profile $D_{\text{H}\beta} = \text{FWHM}(\text{H}\beta)/\sigma_{\text{H}\beta}$, R_{Fe} is the ratio of optical Fe II to $\text{H}\beta$ line flux (e.g. Du et al. 2016a). The value of $D_{\text{H}\beta}$ is 2.35, 3.46, 2.45, 2.83, and 0 for a Gaussian, a rectangular, a triangular, an edge-on rotating ring, and a Lorentzian profile, respectively. $D_{\text{H}\beta}$ depends on the line profile and gives a simple, convenient parameter that may be related to the dynamics of the BLRs (Collin et al. 2006; Du et al. 2016a). R_{Fe} has a correlation with Eigenvector 1 (EV1) from principal component analysis, which has been demonstrated to be driven by the Eddington ratio (Boroson & Green 1992; Sulentic et al. 2000; Boroson 2002; Shen & Ho 2014; Ge et al. 2016).

In this paper, for a large compiled sample of 120 RM AGNs, considering the role of the dimensionless accretion rate $\dot{\mathcal{M}}$, the bivariate correlation of R_{BLR} with L_{5100} and $\dot{\mathcal{M}}$ is investigated. Section 2 presents our sample. Section 3 is data analysis and Section 4 is discussion. Section 5 summaries our results. All of the cosmological calculations in this paper assume $\Omega_{\Lambda} = 0.68$, $\Omega_{\text{M}} = 0.32$, and $H_0 = 67 \text{ km s}^{-1} \text{ Mpc}^{-1}$ (Planck Collaboration et al. 2014).

2 SAMPLE

Up to now, there are 120 RM AGNs with measured $\text{H}\beta$ lags (e.g. Bentz et al. 2013; Du et al. 2015; Grier et al. 2017; Du et al. 2018). We divide them into three subsamples. The first subsample has 25 AGNs presented by SEAMBH collaboration (hereafter SEAMBHs) (Du et al. 2015, 2016b, 2018). These 25 sources were observed by SEAMBH collaboration since 2012. 24 out of 25 are identified to be super-Eddington accretor ($\dot{\mathcal{M}} \geq 3$) (Du et al. 2018). MCG+06-26-012 was selected as a super-Eddington candidate in SEAMBH2012 but was later identified to be a sub-Eddington AGN ($\dot{\mathcal{M}} = 0.46$). The second subsample contains 39 AGNs summarized by Bentz et al. (2013) (excluding Mrk 335 and Mrk 142 again mapped by the SEAMBHs project) and 12 other sources published recently (hereafter BentzSample) (Barth et al. 2015; Bentz et al. 2016a,b; Fausnaugh et al. 2017; Williams et al. 2018). The third subsample contains 44 high- z AGNs ($z \sim 0.1 - 1.0$) from SDSS-RM project which was done by fibre spectrum (hereafter SDSS-RM) (Grier et al. 2017). The entire sample includes 120 AGNs with measured $\text{H}\beta$ lags. We collect $D_{\text{H}\beta}$ and R_{Fe} measured from the optical spectrum, which were suggested to be driven by $\dot{\mathcal{M}}$.

Properties about our sample of 120 AGNs are shown in Table 1. Col. (1) is the source name. Col. (2) is the rest-frame $\text{H}\beta$ lag in units of days. Col. (3) is host-corrected monochromatic luminosity at 5100 Å. Col. (4) is the broad $\text{H}\beta$ FWHM measured from

the mean spectrum. Col. (5) is the broad $H\beta$ line dispersion $\sigma_{H\beta}$ measured from the mean spectrum. Col. (6) is $D_{H\beta}$ and Col.(7) is R_{Fe} . Col.(14) is the reference for these data (e.g. Barth et al. 2013, 2015; Bentz et al. 2006, 2009a,b, 2013, 2014; Collin et al. 2006; Denny et al. 2006, 2010; Du et al. 2015, 2016a,b, 2018; Fausnaugh et al. 2017; Grier et al. 2012, 2017; Ho & Kim 2014; Lu et al. 2016; Pei et al. 2014, 2017; Peterson et al. 2000, 2014; Shen et al. 2015, 2019; Williams et al. 2018; Zhang et al. 2019). The L_{5100} of SDSS-RM sources comes from Shen et al. (2015) and the R_{Fe} is derived from Shen et al. (2019), Col. (2), Col. (4) and Col. (5) come from Grier et al. (2017). For the other sources, Col.(2)-Col. (5), Col.(7) and Col.(11) are mainly from Du et al. (2015) and Du et al. (2016a). For a source with multiple RM measurements, we use the square of measurement error as weight to calculate the weighted average (called the "averaged scheme"). The error of the compiled data is calculated from the weighted average of the measurement errors and the weighted standard deviation. We use the averaged scheme in our analysis like that in Du et al. (2015, 2018).

3 DATA ANALYSIS

3.1 The SMBH mass M_{BH} and the dimensionless accretion rate \dot{M}

We use this sample of 120 RM AGNs with measured $H\beta$ lags to do the bivariate correlation analysis to investigate the effect of \dot{M} in the $R_{BLR}(H\beta) - L_{5100}$ relation. About the downward offset for SEAMBH and SDSS-RM AGNs with respect to the canonical $R_{BLR}(H\beta) - L_{5100}$ relation, the dimensionless accretion rate \dot{M} is suggested to be the key parameter (Du et al. 2016b, 2018). Therefore, we use \dot{M} and L_{5100} to do the bivariate fitting. In this paper, we don't use the Eddington ratio L_{Bol}/L_{Edd} . Given the uncertainty in bolometric corrections, we do not attempt to infer L_{Bol} from the monochromatic luminosity at 5100 Å (e.g. Marconi et al. 2004; Trump et al. 2011; Jin et al. 2012; Wang et al. 2019).

The SMBH masses M_{BH} of 120 broad-line RM AGNs can be derived from the Eq. 1. Here we use three methods to derive M_{BH} and therefore yield three kinds of \dot{M} . Using the $FWHM(H\beta)$ from the mean spectrum to trace the velocity of the BLRs clouds and adopting the virial factor f_{BLR} as 1 (e.g. Du et al. 2016b, 2018), we denote this SMBH mass as $M_{BH,F}$. Using the $\sigma_{H\beta}$ instead of $FWHM(H\beta)$ from the mean spectrum to trace the velocity of the BLRs clouds and adopting f_{BLR} as 4.47 (Woo et al. 2015), we denote this SMBH mass as $M_{BH,\sigma}$. It was found that the line dispersion $\sigma_{H\beta}$ is insensitive to the inclination, while $H\beta$ FWHM has some dependence on the inclination (Collin et al. 2006; Yu et al. 2019). In our previous work (Yu et al. 2019), we proposed a new calibration about the virial factor, the $FWHM(H\beta)$ -based virial factor, has an anti-correlation with the FWHM of the $H\beta$ broad component:

$$\log f_{BLR} = -1.11 \log \frac{FWHM(H\beta)}{2000 \text{ km s}^{-1}} + 0.48. \quad (4)$$

We denote this SMBH mass as $M_{BH,c}$. Therefore we can use three kinds of the M_{BH} to derive \dot{M} , we denote these corresponding \dot{M} as \dot{M}_F , \dot{M}_σ and \dot{M}_c . \dot{M}_F is adopted as the dimensionless accretion rate in the SEAMBHs project (e.g. Du et al. 2016a,b, 2018). In Table 1, Col. (8) is the black hole mass $M_{BH,F}$ derived from the FWHM and $f_{BLR} = 1$. Col. (9) is $M_{BH,\sigma}$ derived from $\sigma_{H\beta}$ and $f_{BLR} = 4.47$ suggested by Woo et al. (2015). Col. (10) is $M_{BH,c}$ derived from FWHM and $f_{BLR} \propto FWHM^{-1.11}$

(Yu et al. 2019). For some AGNs, we use the MCMC (Markov chain Monte Carlo) M_{BH} from the BLR dynamical method, where the virial factor f_{BLR} is directly constrained from velocity-resolved reverberation mapping. (e.g. Li et al. 2018; Pancoast et al. 2018; Williams et al. 2018) (see table 6 in Yu et al. (2019)). Columns (11-13) are the corresponding dimensionless accretion rates \dot{M} . From Equations 4 and 3, assuming $FWHM(H\beta) = 5413 \text{ km s}^{-1}$, then $f_{BLR} = 1$, and $M_{BH,c}$ is the same as $M_{BH,F}$ for a source. Assuming $FWHM(H\beta) = 2000 \text{ km s}^{-1}$, then $f_{BLR} = 3.02$ and $M_{BH,c}$ is larger than $M_{BH,F}$ by 0.48 dex, \dot{M}_c is smaller than \dot{M}_F by 0.96 dex for a source.

In Fig. 1, we show the distributions of three kinds of \dot{M} . The black line is for the first subsample of SEAMBHs AGNs. The green line is for the second subsample of BentzSample. The mean value and the rms of $\log \dot{M}$ are shown in each panel. The blue line is for the third subsample of SDSS-RM AGNs. The subsample of SEAMBHs has the largest mean value of \dot{M} which is expected due to the selection criteria of the sample. The subsample of SDSS-RM has the larger distribution range than the others, which is similarly expected from SDSS sample selection (Shen et al. 2015). For $\log \dot{M}_F$, the mean values with the standard deviations in distributions are 1.68 ± 0.81 , -0.41 ± 1.09 , 0.05 ± 1.38 , respectively for the subsamples of SEAMBHs, BentzSample, SDSS-RM. For $\log \dot{M}_\sigma$, they are respectively 1.17 ± 0.79 , -0.52 ± 0.88 , -0.25 ± 1.30 . For $\log \dot{M}_c$, they are respectively 0.63 ± 0.86 , -0.76 ± 0.86 , -0.25 ± 0.87 . Adopting our FWHM-based f formula (Equation 4), for subsample of SEAMBHs, smaller FWHM leads to larger f_{BLR} . It would lead to larger M_{BH} and thus smaller \dot{M} than for adopting $f_{BLR} = 1$. Adopting the super-Eddington criterion of $\dot{M} \geq 3$ (Du et al. 2018), using \dot{M}_F , there are 24/25, 14/51, 16/44 super-Eddington SMBHs in three subsamples, respectively. Using \dot{M}_σ , there are 20/25, 6/51, 13/44 super-Eddington SMBHs, respectively. Using \dot{M}_c , there are 14/25, 3/51, 12/44 super-Eddington SMBHs, respectively. With \dot{M}_c , the number of super-Eddington sources become smaller. Adopting FWHM-based f in \dot{M}_c , smaller $FWHM(H\beta)$ leads to larger f , and then larger M_{BH} , which makes some AGNs being sub-Eddington. The classification of super-Eddington AGNs depends on the calculation method of M_{BH} and then \dot{M} (see Table 1 1).

In Fig. 2, we find that \dot{M} has correlations with $D_{H\beta}$ and R_{Fe} , which is consistent with the result by Du et al. (2016a). Du et al. (2016a) found that $D_{H\beta} = 2.01 - 0.29 \log \dot{M}_F$, and $R_{Fe} = 0.66 + 0.30 \log \dot{M}_F$. Fig. 3 shows the distributions of $D_{H\beta}$ and R_{Fe} for three subsamples. The SEAMBHs subsample has smaller mean value of $D_{H\beta}$ and has larger mean value of R_{Fe} than other subsamples, which are consistent with their prevalently wide wing and strong Fe II for SEAMBHs sources. Adopting \dot{M}_F , these correlations are stronger than adopting \dot{M}_σ or \dot{M}_c for the entire sample or the sample excluding SDSS-RM AGNs. Adopting \dot{M}_c , the relation between \dot{M}_c and R_{Fe} is weakest. \dot{M}_c has a stronger correlation with $D_{H\beta}$ than R_{Fe} . It is the same as \dot{M}_F . However, \dot{M}_σ has a weaker correlation with $D_{H\beta}$ than R_{Fe} (see values in top left corners in Fig. 2). For the entire sample, the relation of \dot{M} with R_{Fe} or $D_{H\beta}$ becomes weaker than for the sample excluding SDSS-RM AGNs. The SDSS-RM subsample has the larger scatter in all the correlations, with tighter correlations when the SDSS-RM subsample is excluded. Considering the observational uncertainties, this remains true.

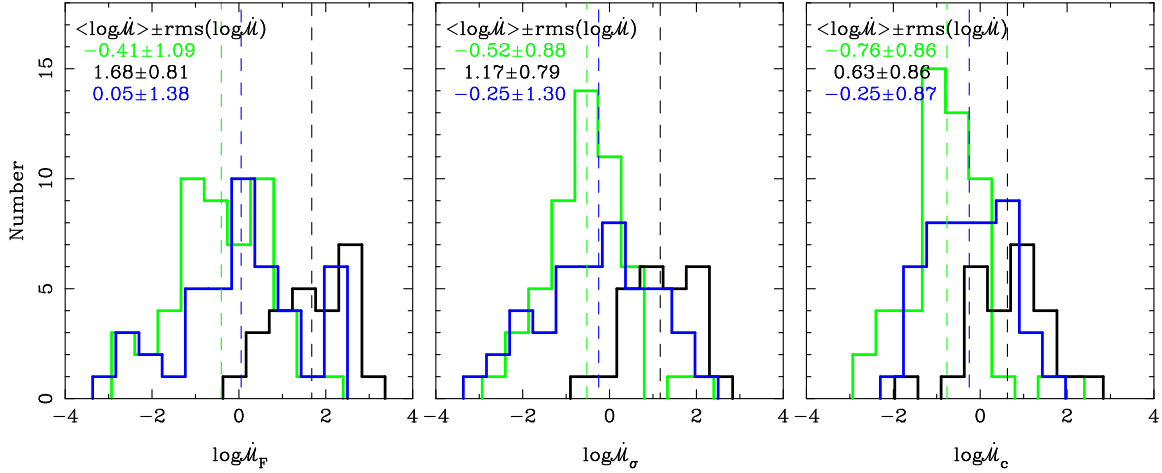


Figure 1. Distributions of three kinds of \dot{M} , i.e., \dot{M}_F , \dot{M}_σ , \dot{M}_c from left to right, respectively. The black, green, blue lines denote the subsamples of SEAMBH, BentzSample, SDSS-RM, respectively. The dash line is the mean value for these three kinds of \dot{M} . The mean value and the rms are shown in the upper left corner of each panel.

3.2 Multivariate liner regression technique

The multivariate regression analysis technique is used to find an extended $R_{\text{BLR}}(\text{H}\beta) - L_{5100}$ relation including other second parameter in the form: $y = \alpha_1 x_1 + \alpha_2 x_2 + \beta_1$. We use the χ^2 as the estimator to find the best values for these fitting parameters (Merloni et al. 2003):

$$\chi^2 = \sum_i \frac{(y_i - \alpha_1 x_{1i} - \alpha_2 x_{2i} - \beta_1)^2}{\sigma_{\text{int}}^2 + \sigma_{y_i}^2 + (\alpha_1 \sigma_{x_{1i}})^2 + (\alpha_2 \sigma_{x_{2i}})^2}, \quad (5)$$

where y_i is the dependent variable. x_{1i} and x_{2i} are the independent variables. σ_{y_i} , $\sigma_{x_{1i}}$ and $\sigma_{x_{2i}}$ are the uncertainties of y_i , x_{1i} and x_{2i} , respectively. σ_{int} is the intrinsic scatter. Because Equation 5 is non-linear in α_1 and α_2 , it is impossible to minimize χ^2 analytically. But for a given set of α_1 and α_2 , we can solve the equation $\frac{\partial \chi^2}{\partial \beta_1} = 0$. Therefore the optimal value $\beta_{1,\text{min}}$ is

$$\beta_{1,\text{min}} = \frac{\sum_i \frac{y_i - \alpha_1 x_{1i} - \alpha_2 x_{2i}}{\sigma_{\text{int}}^2 + \sigma_{y_i}^2 + (\alpha_1 \sigma_{x_{1i}})^2 + (\alpha_2 \sigma_{x_{2i}})^2}}{\sum_i \frac{1}{\sigma_{\text{int}}^2 + \sigma_{y_i}^2 + (\alpha_1 \sigma_{x_{1i}})^2 + (\alpha_2 \sigma_{x_{2i}})^2}}, \quad (6)$$

The intrinsic scatter σ_{int} in Equation 5 is allowed to vary as an effective additional y error by repeating the fit until one obtains $\chi_r^2 = 1$ where $\chi_r^2 = \chi^2 / N_{\text{dof}}$, N_{dof} is the number of degree of freedom. The value of σ_{int} can be derived by iteration (Bamford et al. 2006; Bedregal et al. 2006; Park et al. 2012). In the first step set the $\sigma_{\text{int}} = 0$ and compute the χ_r^2 . If $\chi_r^2 \leq 1$ then $\sigma_{\text{int}} = 0$. If $\chi_r^2 > 1$ then set a initial value for the $\sigma_{\text{int},1}$ and do the iteration (Bamford et al. 2006; Bedregal et al. 2006; Park et al. 2012):

$$\sigma_{\text{int},j+1}^2 = \sigma_{\text{int},j}^2 \chi_r^{2\alpha}, \alpha > 0. \quad (7)$$

In this iteration, we adopt $\alpha = 2/3$. When $\chi_r^2 > 1$, $\sigma_{\text{int},j}^2$ is too small and thus should be increased for the next iteration. When $\chi_r^2 < 1$, $\sigma_{\text{int},j}^2$ is too large and should be decreased for the next iteration. When $\chi_r^2 = 1$, $\sigma_{\text{int},j+1}^2 = \sigma_{\text{int},j}^2$ and the value of $\sigma_{\text{int},j}$ is what we want.

The bootstrap method is used to estimate the error bars of α_1 , α_2 , β and σ_{int} . We resampled the data for 100 times and repeated the multiple linear regressions like above. Therefore we can derive 100 values for each parameters. For each parameter, we sort these values, adopt the 16th and 84th values as endpoints of the 1σ confidence interval, and calculate its error.

3.3 An extended $R_{\text{BLR}}(\text{H}\beta) - L_{5100}$ relation including the dimensionless accretion rate \dot{M}

Because the SDSS-RM lags are computed from JAVELIN, which typically gives smaller uncertainties than the ICCF lags used in the other two subsamples (e.g. Yu et al. 2019), we simply use the canonical $R_{\text{BLR}}(\text{H}\beta) - L_{5100}$ relation derived by sub-Eddington AGNs for our sample excluding SDSS-RM AGNs with the fibre spectra. Fig. 4 shows the $R_{\text{BLR}}(\text{H}\beta) - L_{5100}$ relation for our sample. The solid line is defined by the Equation 2, where $\alpha = 33.88$ light days and $\beta = 0.51$ for sub-Eddington AGNs ($\dot{M}_F < 3$) from our sample excluding SDSS-RM AGNs, which is almost the same as Du et al. (2018). We adopted it as the canonical $R_{\text{BLR}}(\text{H}\beta) - L_{5100}$ relation. For our sample excluding SDSS-RM AGNs, the Spearman correlation coefficient $r_s = 0.837$, the probability of the null hypothesis $p_{\text{null}} = 0.45 \times 10^{-20}$, and the offset rms (with respect to the canonical $R_{\text{BLR}}(\text{H}\beta) - L_{5100}$ relation) is 0.31 dex. For our entire sample, $r_s = 0.731$, $p_{\text{null}} = 0.24 \times 10^{-20}$, and the offset rms is 0.35 dex. For subsamples of SEAMBH AGNs and SDSS-RM AGNs, there is a downward offset with respect to the solid line. Using \dot{M}_F , the mean value of the offset from the canonical $R_{\text{BLR}}(\text{H}\beta) - L_{5100}$ relation is respectively -0.36 dex, -0.16 dex, -0.48 dex, and -0.34 dex for super-Eddington accretion SMBHs in three subsamples (SEAMBHs, BentzSample, SDSS-RM), and entire sample. Using \dot{M}_σ , the values are -0.42 dex, -0.37 dex, -0.42 dex, -0.41 dex, respectively. Using \dot{M}_c , the values are -0.55 dex, -0.46 dex, -0.59 dex, -0.55 dex, respectively. It is found that super-Eddington AGNs has a negative mean offset with respect to the canonical $R_{\text{BLR}}(\text{H}\beta) - L_{5100}$ relation for sub-Eddington AGNs, no matter what kind of \dot{M} . Particularly for the BentzSample subsample, the offset of 14/51 super-Eddington accretion SMBHs is smallest (-0.16 ± 0.28 dex, statistically marginal) for the simple FWHM-based \dot{M}_F , and there is only three super-Eddington AGNs with offset of -0.46 dex for the corrected-FWHM \dot{M}_c .

Considering the deviation $\Delta R_{\text{BLR}}(\text{H}\beta)$ from the canonical $R_{\text{BLR}}(\text{H}\beta) - L_{5100}$ relation defined by sub-Eddington AGNs, it was suggested that objects with $\dot{M} < 3$ would be associated with $\Delta R_{\text{BLR}}(\text{H}\beta) \sim 0$, while objects with $\dot{M} \geq 3$ the deviation would decrease as a function with \dot{M} (Du et al. 2016b, 2018). Since some super-Eddington AGNs deviate from the canonical

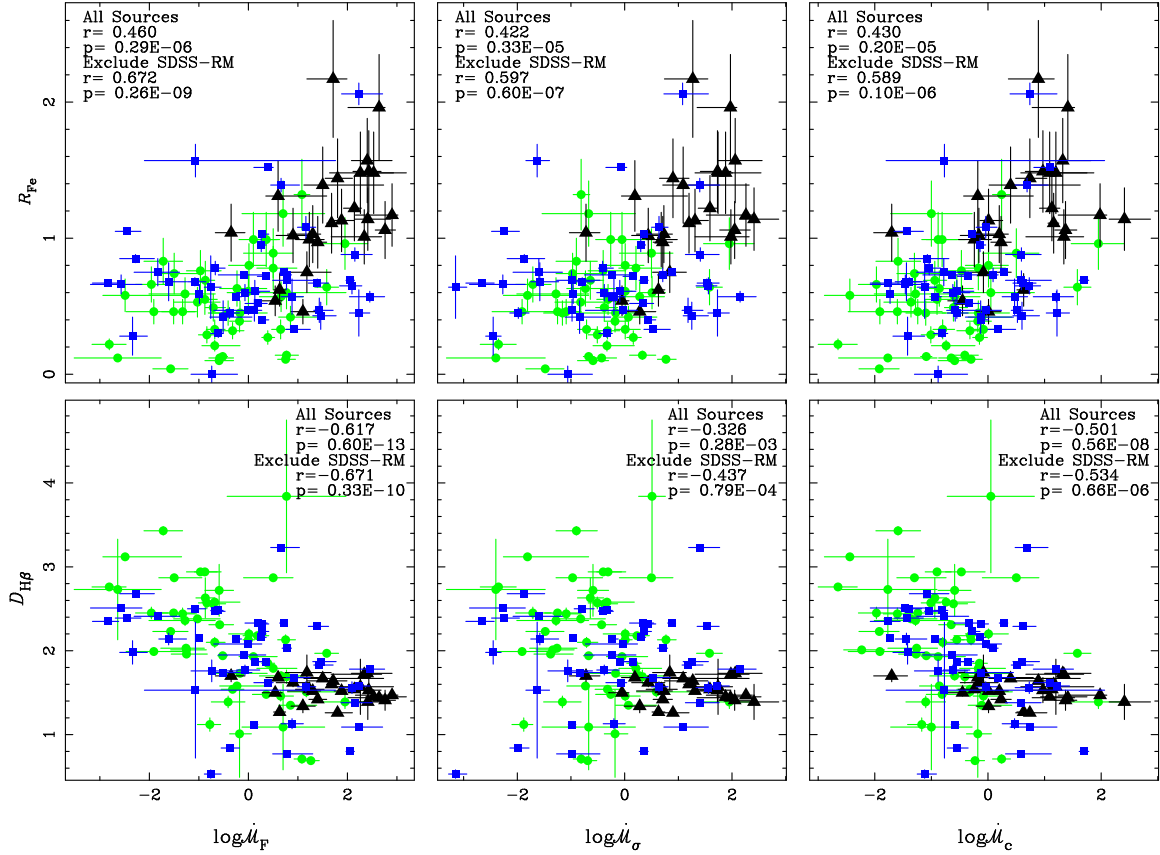


Figure 2. Correlations of \dot{M} with R_{Fe} (top) and $D_{\text{H}\beta}$ (bottom). In the left two panels, the dimensionless accretion rate \dot{M}_F is derived from FWHM and the virial factor $f_{\text{BLR}}=1$. In the middle two panels, \dot{M}_σ is derived from $\sigma_{\text{H}\beta}$ and $f_{\text{BLR}}=4.47$. In the right two panels, \dot{M}_c is derived from FWHM and the FWHM-based factor $f_{\text{BLR}} \propto \text{FWHM}^{-1.11}$. The source in the subsample of SEAMBHs is shown as a black triangle. The source in the subsample of BentzSample is shown as a green circle. The source in the subsample of SDSS-RM is shown as a blue square. The correlation coefficient r_s and the null possibility p_{null} are shown in the left/right corner in each panel.

$R_{\text{BLR}}(\text{H}\beta) - L_{5100}$ relation, it is necessary to give a new extended $R_{\text{BLR}}(\text{H}\beta) - L_{5100}$ relation. Considering \dot{M} as the key parameter (Du et al. 2018; Martínez-Aldama et al. 2019), we use the multivariate liner regression technique as described in Section 3.2 to find an extended $R_{\text{BLR}}(\text{H}\beta) - L_{5100}$ relation, i.e., the correlation between $R_{\text{BLR}}(\text{H}\beta)$, L_{5100} and \dot{M} . For three kinds of \dot{M} and excluding SDSS-RM or not, we perform the bivariate liner regressions respectively and present the results in Table 2. Including the dimensionless accretion rate \dot{M} , the relations in Fig. 5 become stronger (see Table 2).

In Fig. 5, we present the dependence of the $R_{\text{BLR}}(\text{H}\beta)$ on the L_{5100} and \dot{M} . Three top panels are for our sample excluding the SDSS-RM sources and three bottom panels are for all sources. In two left panels, \dot{M} is derived from the H β FWHM and $f_{\text{BLR}} = 1$. In two middle panels, \dot{M} is derived from $\sigma_{\text{H}\beta}$ and $f_{\text{BLR}}=4.47$. In two right panels, \dot{M} is derived from the H β FWHM and the FWHM-based factor $f_{\text{BLR}} \propto \text{FWHM}^{-1.11}$. When the SDSS-RM sources are included, the significance of the correlation decreases (shown in right panels in 5). Including \dot{M} in the $R_{\text{BLR}}(\text{H}\beta) - L_{5100}$ relation, the correlations become stronger than the canonical $R_{\text{BLR}}(\text{H}\beta) - L_{5100}$ relation and smaller values of the offset rms (see Fig. 4), especially for \dot{M}_c derived from our virial factor calibration (Yu et al. 2019). Adopting \dot{M}_c , for excluding the SDSS-RM AGNs, the intrinsic scatter is $\sigma_{\text{int}} = 0.05$ dex, R_{BLR} offset rms (with respect to this relation) is 0.18 dex, $r_s = 0.952$ and $p_{\text{null}} = 0.12 \times 10^{-43}$. For all RM AGNs, σ_{int} is 0.13 dex, the

R_{BLR} offset rms is 0.21 dex, $r_s = 0.883$ and $p_{\text{null}} = 0.16 \times 10^{-44}$. Adopting \dot{M}_c , an order of magnitude in \dot{M}_c would lead to a change of 0.31 dex in $\log R_{\text{BLR}}$ for the bivariate relation shown in the bottom left panel shown in Fig. 5. Adopting \dot{M}_F or \dot{M}_σ , an order of magnitude in \dot{M} would lead to a change of 0.14 dex or 0.21 dex in $\log R_{\text{BLR}}$ for the bivariate relation shown in the top left panel or middle left panel shown in Fig. 5. There are large range of \dot{M} for AGNs from hot accretion to standard accretion to super-Eddington accretion (Yuan & Narayan 2014). Therefore, the role of \dot{M} in the $R_{\text{BLR}}(\text{H}\beta) - L_{5100}$ relation would be important (see additional discussion in section 4).

3.4 An extended $R_{\text{BLR}}(\text{H}\beta) - L_{5100}$ relation including the observational parameter R_{Fe} or $D_{\text{H}\beta}$

The dimensionless accretion rate \dot{M} is computed directly from the continuum L_{5100} and also (for most sources) from R_{BLR} (see equation 3). This means that any comparison of \dot{M} with the other quantities suffers from self-correlation. R_{Fe} and the H β shape $D_{\text{H}\beta}$ are measures of \dot{M} that are independent of R_{BLR} and L_{5100} . These two observational parameters of R_{Fe} and $D_{\text{H}\beta}$ can be measured from the single-epoch spectrum. In section 3.1, it is found that R_{Fe} or $D_{\text{H}\beta}$ has a relation with \dot{M} (see Fig. 2). Therefore, we use the multivariate regression analysis technique to investigate the extended $R_{\text{BLR}}(\text{H}\beta) - L_{5100}$ relation including obser-

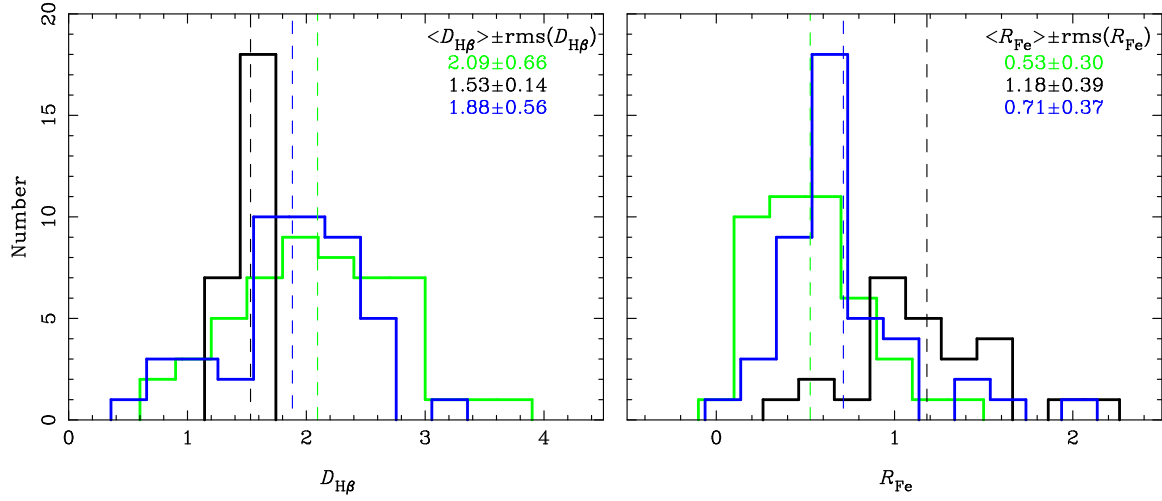


Figure 3. The distribution of $D_{H\beta}$ (left) and R_{Fe} (right) for three subsamples. The mean value and the rms are shown in the upper left corner of each panel. The black, green, blue lines denote the subsamples of SEAMBHs, BentzSample, and SDSS-RM, respectively.

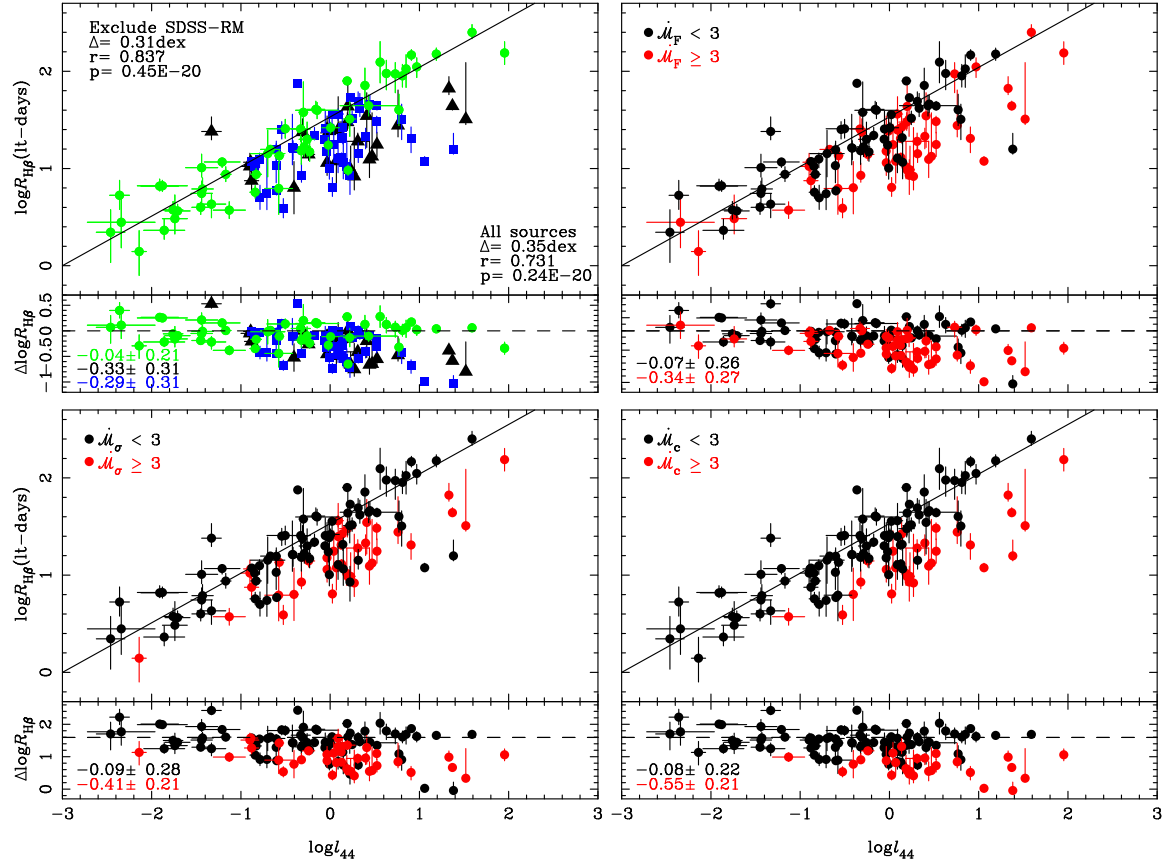


Figure 4. Left top: the $R_{BLR}(H\beta) - l_{44}$ relation for BentzSample (green circles), SEAMBH (black triangles) and SDSS-RM (blue squares). The solid line corresponds to the $R_{BLR}(H\beta) - l_{44}$ relation from Equation 2 and $\alpha = 33.88$ light days and $\beta = 0.51$ (Du et al. 2018) for super-Eddington AGNs. The rms respect to the solid line, the Spearman correlation coefficient r_s and probability of the null hypothesis p_{null} are shown in the upper left/right corner. The values of the mean and the standard deviation are shown in the left corner. Right top: the same $R_{BLR}(H\beta) - l_{5100}$ relation as the left panels for super-Eddington AGNs (red circles) and sub-Eddington AGNs (black circles) with the criterion of $\mathcal{M}_F \geq 3$. Left bottom: the same as the top right panel but for \mathcal{M}_σ . Right bottom: the same as the top right panel but for \mathcal{M}_c .

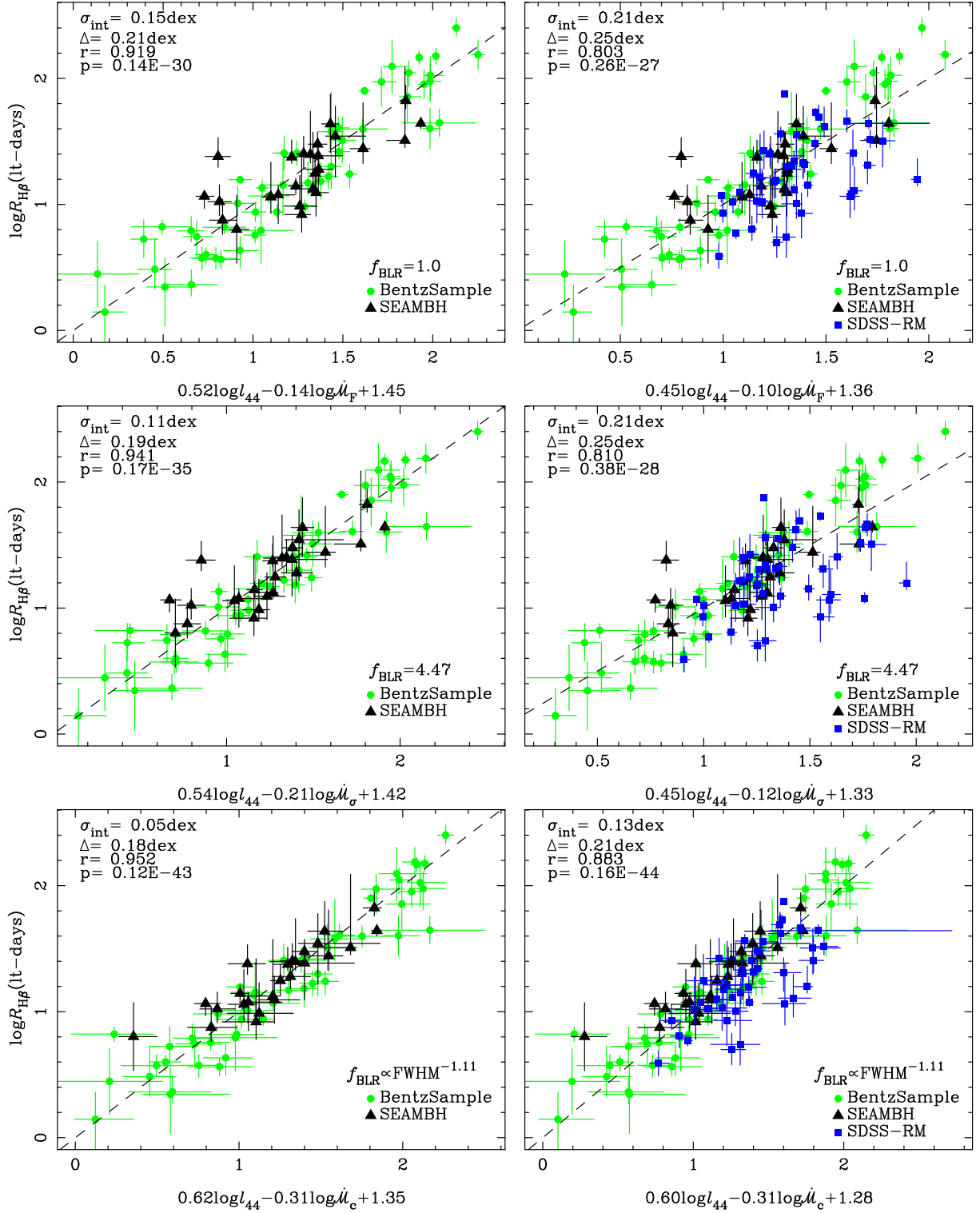


Figure 5. Dependence of the $R_{\text{BLR}}(\text{H}\beta)$ on the l_{44} and the \dot{M} . The left panels demonstrate the dependence for all the RM AGNs excluding the SDSS-RM AGNs. The right panels demonstrate the dependence for all the RM AGNs. The symbols are the same to the Fig. 2. The dash line is 1:1. In the top two panels, the dimensionless accretion rate is derived from FWHM and the virial factor $f_{\text{BLR}}=1.0$. In the middle two panels, the dimensionless accretion rate is derived from $\sigma_{\text{H}\beta}$ and $f_{\text{BLR}}=4.47$. In the bottom two panels, the dimensionless accretion rate is derived from FWHM and the virial factor $f_{\text{BLR}} \propto \text{FWHM}^{-1.11}$. The intrinsic scatter, the offset rms respect to the solid line, the Spearman correlation coefficient r_s and probability of the null hypothesis p_{null} are shown in the left corner in each panel.

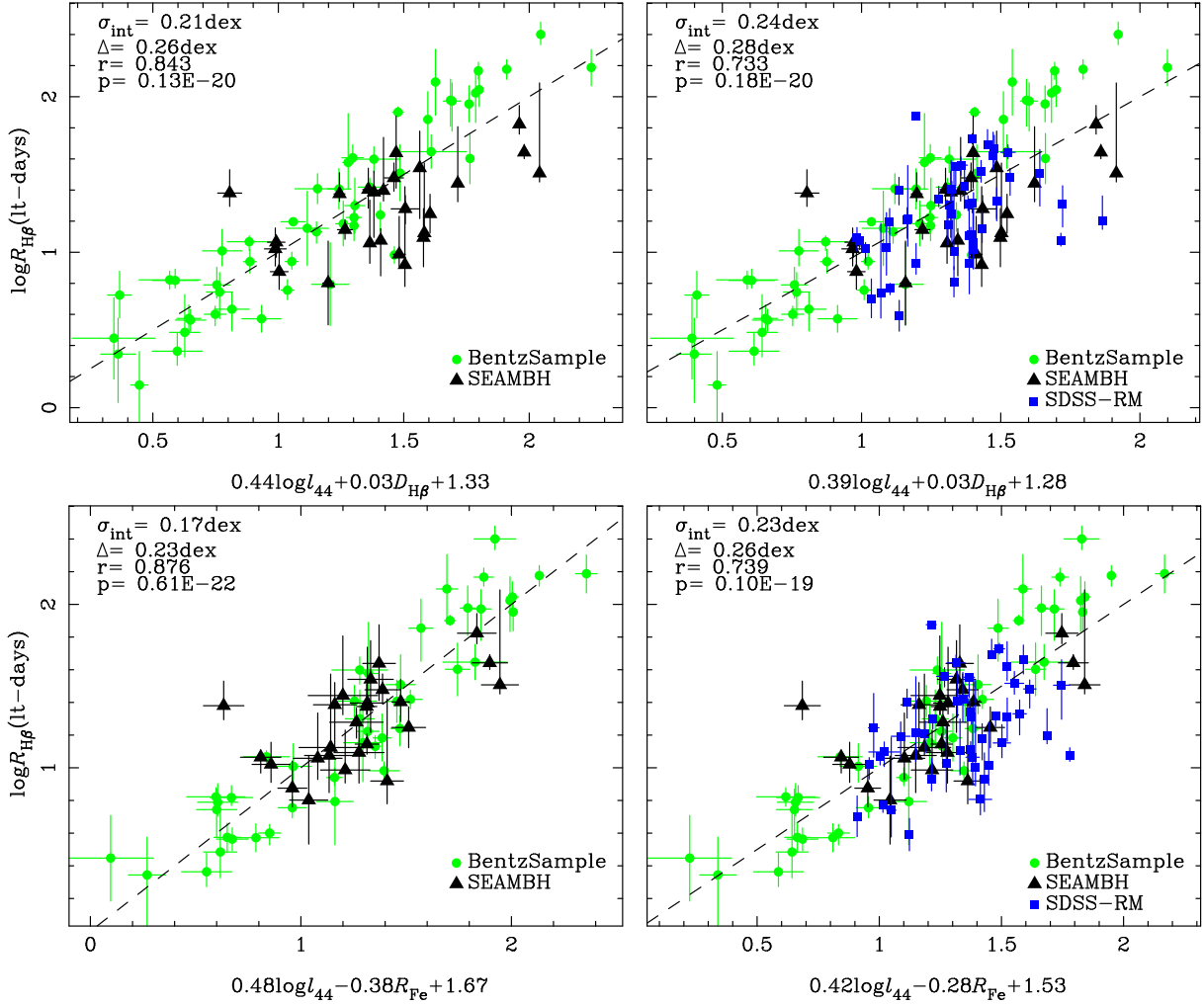


Figure 6. Dependence of the $R_{\text{BLR}}(\text{H}\beta)$ on the l_{44} and the $D_{\text{H}\beta}$ (top). Dependence of the $R_{\text{BLR}}(\text{H}\beta)$ on the l_{44} and the R_{Fe} (bottom). Two left panels demonstrate the dependence for all the RM AGNs excluding the SDSS-RM AGNs and two right panels demonstrate the dependence for all the RM AGNs. The symbols are the same to the Fig. 2. The dash line is 1:1. The intrinsic scatter, the offset rms respect to the solid line, the Spearman correlation coefficient r_s and probability of the null hypothesis p_{null} are shown in the left corner in each panel.

vational parameters, i.e., R_{Fe} and $D_{\text{H}\beta}$. In Fig. 6, new empirical $R_{\text{BLR}}(\text{H}\beta) - L_{5100}$ relations are presented including R_{Fe} or $D_{\text{H}\beta}$. Excluding SDSS-RM AGNs, the extended $R_{\text{BLR}}(\text{H}\beta) - L_{5100}$ relations are

$$\begin{aligned} \log R_{\text{BLR}}(\text{H}\beta) &= (0.48 \pm 0.03) \log l_{44} - (0.38 \pm 0.04) R_{\text{Fe}} \\ &\quad + (1.67 \pm 0.09) \text{ ltd}, \\ \log R_{\text{BLR}}(\text{H}\beta) &= (0.44 \pm 0.03) \log l_{44} - (0.03 \pm 0.04) D_{\text{H}\beta} \\ &\quad + (1.33 \pm 0.08) \text{ ltd}. \end{aligned} \quad (8)$$

For the subsample of excluding SDSS-RM AGNs, in an extended $R_{\text{BLR}}(\text{H}\beta) - L_{5100}$ relation including R_{Fe} , $r_s = 0.876$, $p_{\text{null}} = 0.61 \times 10^{-22}$. Including $D_{\text{H}\beta}$, $r_s = 0.843$, $p_{\text{null}} = 0.13 \times 10^{-20}$. Including R_{Fe} or $D_{\text{H}\beta}$ in the $R_{\text{BLR}}(\text{H}\beta) - L_{5100}$ relation, r_s increase with respect to that for the $R_{\text{BLR}}(\text{H}\beta) - L_{5100}$ relation ($r_s = 0.837$, $p_{\text{null}} = 0.45 \times 10^{-20}$) shown in Fig. 4. The offset rms decreases from 0.31 dex to 0.26 dex (including $D_{\text{H}\beta}$) or 0.23 dex (including R_{Fe}). For the entire sample, in this extended relation including R_{Fe} or $D_{\text{H}\beta}$, $r_s = 0.733$ (for $D_{\text{H}\beta}$) or $r_s = 0.739$ (for R_{Fe}), which is slightly larger than $r_s = 0.731$ for the $R_{\text{BLR}}(\text{H}\beta) - L_{5100}$ relation for the entire sample (see Fig.

4). The offset rms decreases from 0.35 dex to 0.28 dex (including $D_{\text{H}\beta}$) or 0.26 dex (including R_{Fe}).

Although the extended $R_{\text{BLR}}(\text{H}\beta) - L_{5100}$ relations become weaker for the entire sample than for the subsample excluding SDSS-RM AGNs, the extended $R_{\text{BLR}}(\text{H}\beta) - L_{5100}$ relations including R_{Fe} and $D_{\text{H}\beta}$ become stronger than for the $R_{\text{BLR}}(\text{H}\beta) - L_{5100}$ relation shown in Fig. 4. Including R_{Fe} , the improvement of $R_{\text{BLR}}(\text{H}\beta) - L_{5100}$ relation is more significant than for including $D_{\text{H}\beta}$ (the y-axis offset rms is 0.23 dex versus 0.26 dex). A change of 1 in R_{Fe} would lead to a change of 0.38 dex in $\log R_{\text{BLR}}$ for the bivariate relation shown in the bottom left panel in Fig. 6. Considering a slope of 0.03 ± 0.04 for the $\text{H}\beta$ shape $D_{\text{H}\beta}$, it should be noted that the best-fit relation with $D_{\text{H}\beta}$ shows only a marginal dependence on this quantity (i.e., a slope that 1σ different from zero). R_{Fe} is a better "fix" for the $R_{\text{BLR}}(\text{H}\beta) - L_{5100}$ offset than the $\text{H}\beta$ shape $D_{\text{H}\beta}$. Including SDSS-RM AGNs, a change of 1 in R_{Fe} would lead to a smaller change of $\log R_{\text{BLR}}$, from 0.38 dex to 0.28 dex. R_{Fe} has more contribution in $R_{\text{BLR}}(\text{H}\beta) - L_{5100}$ relation than for $D_{\text{H}\beta}$. It is consistent well with the result by Du & Wang (2019). Considering the correlations of \mathcal{M}_{F} with R_{Fe} or $D_{\text{H}\beta}$ found by Du et al.

(2016a), from Eq. 8 we can derive that $R_{\text{BLR}} \propto l_{44}^{0.49} \dot{\mathcal{M}}_{\text{F}}^{0.114}$, or $R_{\text{BLR}} \propto l_{44}^{0.45} \dot{\mathcal{M}}_{\text{F}}^{0.023}$. They have some slight difference comparing with the equations shown in the top left panel in Fig. 5. It is due to large scatter when using R_{Fe} or $D_{\text{H}\beta}$ to substitute $\dot{\mathcal{M}}$.

4 DISCUSSION

4.1 The $R_{\text{BLR}}(\text{H}\beta) - L_{5100}$ relation: scatter and origin

Considering the photonization model of the BLRs in AGNs (Ferland & Netzer 1983), the ionization parameter $U = \frac{Q(\text{H})}{n_e 4\pi R^2 c}$, where R is the BLRs size for the $\text{H}\beta$ broad line, c is the speed of light, n_e is the electron number density, and $Q(\text{H}) = \int_{13.6\text{eV}}^{\infty} \frac{L_{\nu}}{h\nu} d\nu$ is the flux of hydrogen ionizing photons emitted by the central source. The ionization level of the BLR clouds can be estimated using either the ionizing flux L_{ion} at 912\AA , or Q (e.g. Wang et al. 2014a; Czerny et al. 2019). Adopting some assumptions, such as the point central ionization source, the same U , the same n_e , the same SED, and the same BLRs geometry, we can derive $R_{\text{BLR}} \propto Q(\text{H})^{0.5} \propto L_{5100}^{0.5}$, i.e., the $R_{\text{BLR}}(\text{H}\beta) - L_{5100}$ relation. The UV/optical luminosity ratio depends on detail SMBH accretion process, which can be used to explain the shorter lags than that expected from the canonical $R_{\text{BLR}}(\text{H}\beta) - L_{5100}$ relation (Wang et al. 2014a; Czerny et al. 2019). It is also possible for different values of U or n_e for different AGNs.

The change in SED with the luminosity is suggested that brighter AGNs have flatter optical-UV continua, ranging from an average slope (α in $f_{\nu} \propto \nu^{\alpha}$) of about -1 for Seyfert galaxies to about -0.3 for quasars (although host-correction is a problem) (e.g. Kaspi et al. 2005). Quasars have a larger UV/optical luminosity ratio than Seyfert galaxies. Using UV luminosity to substitute the optical luminosity, the slope of the BLR size versus luminosity relation becomes shallower (Kaspi et al. 2005). Ho (2008) also gave the different slope of the optical-UV continuum binned by the Eddington ratio, and found large UV/optical luminosity ratio for nearby AGNs with large Eddington ratios (see their Fig. 7). For our result of the $\dot{\mathcal{M}}$ role in the $R_{\text{BLR}}(\text{H}\beta) - L_{5100}$ relation, larger $\dot{\mathcal{M}}$ leads to smaller R_{BLR} at fixed L_{5100} (see Fig. 5). AGNs with large luminosity or large $\dot{\mathcal{M}}$ always have large UV/optical luminosity ratio, which leads to a relatively large BLR size. Therefore, it is difficult to explain the smaller R_{BLR} at fixed L_{5100} , especially for bright SEAMBHs.

For different SMBH spins, M_{BH} , and $\dot{\mathcal{M}}$, the theoretical UV/optical luminosity ratio were calculated from the general relativistic version of the Shakura & Sunyaev (1973) disk (Wang et al. 2014a; Czerny et al. 2019). For AGNs with larger Eddington ratio, smaller M_{BH} , large spin, the relation between L_{ion} and L_{5100} is almost linear. For other conditions, the temperature of the accretion disk drops to make the SED peak moving into UV band, leading to a non-linear relation between L_{ion} and L_{5100} . Large black hole mass, low Eddington ratio and low spin lead to significant differences in the slope of the optical-UV continuum (Ho 2008; Trump et al. 2011; Lusso et al. 2012). The retrograde spin leads to a cold accretion disk and makes large scatter in the $R_{\text{BLR}}(\text{H}\beta) - L_{5100}$ relation. Therefore, for the smaller R_{BLR} at fixed L_{5100} , the reason is small Eddington ratio or small SMBH spin, which lead to a cold disk, and a deficit of ionizing photons in the BLR. For SEAMBHs with largest $\dot{\mathcal{M}}$, the self-shadowing effects from a slim disk would lead to a deficit of ionizing photons illuminating BLR clouds (Wang et al. 2014a,b). Therefore, the SED changes, connected to changes in $\dot{\mathcal{M}}$, are the most likely culprit

for the breadth in the $R_{\text{BLR}}(\text{H}\beta) - L_{5100}$ relation in the first-order consideration.

It is also noted that there are some scatter in our extended $R_{\text{BLR}}(\text{H}\beta) - L_{5100}$ relation including $\dot{\mathcal{M}}$. In Fig. 5 and Fig. 6, it is found that the correlations become weaker when including SDSS-RM quasars. There exists the excess $R_{\text{BLR}}(\text{H}\beta) - L_{5100}$ scatter of the SDSS-RM quasars. The SDSS-RM subsample is less well explained by the extended $R_{\text{BLR}}(\text{H}\beta) - L_{5100}$ relations than are the subsamples of BentzSample and SEAMBHs. One reason is that the SDSS-RM lags are computed from JAVELIN, which typically gives smaller uncertainties than the ICCF lags used in the other two samples. The other is possibly due to the luminosity-threshold (Shen et al. 2015) or the retrograde spin for SDSS-RM subsample (Du et al. 2018).

Our result of the dependence of the $R_{\text{BLR}}(\text{H}\beta) - L_{5100}$ relation on $\dot{\mathcal{M}}$ supports that R_{BLR} has a relation with the accretion process. Using the multivariate regression analysis technique, for the entire sample, we also find the relation of R_{BLR} with M_{BH} and $\dot{\mathcal{M}}$, i.e., $R_{\text{BLR}} \propto M_{\text{BH}}^{0.61} \dot{\mathcal{M}}_{\text{F}}^{0.20}$ ($r_s = 0.774$), $R_{\text{BLR}} \propto M_{\text{BH}}^{0.61} \dot{\mathcal{M}}_{\sigma}^{0.18}$ ($r_s = 0.787$), $R_{\text{BLR}} \propto M_{\text{BH}}^{0.85} \dot{\mathcal{M}}_{\text{c}}^{0.09}$ ($r_s = 0.876$). For a simple model of gravitational instability of the standard accretion disk leading the formation of the BLRs clouds (Bian & Zhao 2002), $R_{\text{BLR}} \propto L_{5100}^{0.5} \dot{M}^{-37/45} \propto M_{\text{BH}}^{-7/45} \dot{\mathcal{M}}^{-22/45}$. Therefore, our measured accretion rate dependence is not consistent with the simple model of the gravitational instability of accretion disk as the origin of the BLRs. It was found that the size of torus dust is about 4 times of the BLRs size from the optical/near-infrared RM (e.g. Kokubo & Minezaki 2019). The BLR may instead form from the inner edge of the torus (e.g. Wang et al. 2017), or from some other means in which BLR size is positively correlated with accretion rate and the SMBH mass.

4.2 The extended empirical $R_{\text{BLR}}(\text{H}\beta) - L_{5100}$ relation: R_{Fe} or $D_{\text{H}\beta}$

It was found that EV1 is driven by the accretion rate (e.g. Boroson 2002). From the optical spectra of AGNs, we use two EV1-related parameters of R_{Fe} and $D_{\text{H}\beta}$ to substitute $\dot{\mathcal{M}}$. In Fig. 2, both R_{Fe} and $D_{\text{H}\beta}$ seem to effectively correlate with $\dot{\mathcal{M}}$. From Fig. 3, R_{Fe} has a wide distribution than $D_{\text{H}\beta}$, which is around 2. For the distribution of R_{Fe} , the ratios of the mean value to the rms is 3.03, 1.92, 1.77, respectively for three subsamples of SEAMBHs, SDSS-RM, BentzSample. For the distribution of $D_{\text{H}\beta}$, the ratios of the mean value to the rms is 10.93, 3.36, 3.17, respectively for these three subsamples. For the subsample of SEAMBHs, the R_{Fe} has a wide distribution and $D_{\text{H}\beta}$ has a narrow distribution. The wide distribution of R_{Fe} than $D_{\text{H}\beta}$ possibly leads to that the $\text{H}\beta$ shape $D_{\text{H}\beta}$ less correlates with $R_{\text{BLR}}(\text{H}\beta) - L_{5100}$ offset than R_{Fe} (see Fig. 6). R_{Fe} is a better "fix" for the $R_{\text{BLR}}(\text{H}\beta) - L_{5100}$ offset than $D_{\text{H}\beta}$. This empirical $R_{\text{BLR}}(\text{H}\beta) - L_{5100}$ relation including R_{Fe} would be used to derive the BLR size for the $\text{H}\beta$ broad line instead of the canonical $R_{\text{BLR}}(\text{H}\beta) - L_{5100}$ relation, and then weigh M_{BH} from the single-epoch spectrum.

5 CONCLUSIONS

For a compiled sample of 120 RM AGNs, the dependence of the $R_{\text{BLR}}(\text{H}\beta) - L_{5100}$ relation on $\dot{\mathcal{M}}$ is investigated. Using observational parameters of R_{Fe} and $D_{\text{H}\beta}$, extended empirical $R_{\text{BLR}} - L_{5100}$ relations are presented, which can be used to calcu-

late the BLRs sizes from a single-epoch spectrum. The main conclusions are summarized as follows:

- Using our recently calibrated virial factor f , and the velocity tracer from the $H\beta$ FWHM or the line dispersion $\sigma_{H\beta}$ from the mean spectrum, three kinds of SMBH masses M_{BH} and the dimensionless accretion rates \dot{M} are calculated for a large compiled sample of 120 RM AGNs. The classification of super-Eddington AGNs depends on the calculation method of M_{BH} and thus \dot{M} . It is found that R_{Fe} or $D_{H\beta}$ has a relation with \dot{M} .

- Including the effect of \dot{M} , the bivariate correlation of R_{BLR} with L_{5100} and \dot{M} has a smaller scatter than that for the canonical $R_{BLR}(H\beta) - L_{5100}$ relation. The correlation coefficient r_s is larger and p_{null} is smaller than the canonical $R_{BLR}(H\beta) - L_{5100}$ relation. For M_{BH} and \dot{M} derived from $H\beta$ FWHM and $H\beta$ FWHM-based f , the bivariate correlation of R_{BLR} with L_{5100} and \dot{M}_F has a smallest scatter for three cases of \dot{M} .

- Substituting observational parameter of R_{Fe} or $D_{H\beta}$ for \dot{M} , extended empirical $R_{BLR}(H\beta) - L_{5100}$ relations are found, which would be used to derive R_{BLR} instead of by the canonical $R_{BLR}(H\beta) - L_{5100}$ relation, and then M_{BH} from the single-epoch spectrum. Including the optical Fe II relative ratio R_{Fe} , the improvement of $R_{BLR}(H\beta) - L_{5100}$ relation is more significant than for including the line profile parameter $D_{H\beta}$. R_{Fe} is a better "fix" for the $R_{BLR}(H\beta) - L_{5100}$ offset than the $H\beta$ shape $D_{H\beta}$. The best relation is $\log R_{BLR} = (0.42 \pm 0.03) \log l_{44} - (0.28 \pm 0.04) R_{Fe} + (1.53 \pm 0.08) \text{ ltd}$ for the entire sample, with an intrinsic scatter of 0.23 dex.

- Although our measured accretion rate dependence is not consistent with the simple model of the accretion disk instability leading the BLRs formation, our results show that the accretion rate has an important role in the $R_{BLR}(H\beta) - L_{5100}$ relation. The BLR may instead form from the inner edge of the torus, or from some other means in which BLR size is positively correlated with accretion rate and the SMBH mass.

ACKNOWLEDGEMENTS

We are also very grateful to the anonymous referee for her/his instructive comments which significantly improved the content of the paper. This work is supported by the National Key Research and Development Program of China (No. 2017YFA0402703). This work has been supported by the National Science Foundations of China (Nos. 11973029 and 11873032).

REFERENCES

Barth A. J., et al., 2013, *ApJ*, 769, 128
 Barth A. J., Bennert V. N., Canalizo G., et al., 2015, *ApJS*, 217, 26
 Bamford S. P., Aragón-Salamanca A., Milvang-Jensen B., 2006, *MNRAS*, 366, 308
 Bedregal A. G., Aragón-Salamanca A., Merrifield M. R., et al., 2006, *MNRAS*, 373, 1125
 Bentz M. C., et al., 2006, *ApJ*, 651, 775
 Bentz M. C., et al., 2009a, *ApJ*, 705, 199
 Bentz M. C., et al., 2009a, *ApJ*, 697, 160
 Bentz M. C., et al., 2013, *ApJ*, 767, 149
 Bentz M. C., et al., 2014, *ApJ*, 796, 8
 Bentz M. C., et al., 2016a, *ApJ*, 830, 136
 Bentz M. C., Batista M., Seals J., 2016b, *ApJ*, 831, 2
 Bian W.-H., Zhao Y.-H., 2002, *A&A*, 395, 465
 Bian W.-H., Zhao Y.-H., 2004, *MNRAS*, 347, 607

Bian W.-H., Hu C., Gu Q.-S., Wang J.-M., 2008, *MNRAS*, 390, 752
 Blandford R., McKee C., 1982, *ApJ*, 255, 419
 Boroson T. A., Green R. F., 1992, *ApJS*, 80, 109
 Boroson T. A., 2002, *ApJ*, 565, 78
 Collin S., Kawaguchi T., Peterson B., Vestergaard M., 2006, *A&A*, 456, 75
 Czerny B., et al., 2019, *ApJ*, 870, 84, preprints (arXiv: 1811.09559)
 Davis S. W., & Laor A., 2011, *ApJ*, 728, 98
 Denny K. D., et al., 2006, *ApJ*, 653, 152
 Denny K. D., et al., 2010, *ApJ*, 721, 715
 Du P., et al., 2015, *ApJ*, 806, 22
 Du P., et al., 2016a, *ApJ*, 818, L14
 Du P., et al., 2016b, *ApJ*, 825, 126
 Du P., et al., 2018, *ApJ*, 856, 6
 Du P., Wang J.-M., 2019, *ApJ*, arxiv: 1909.06735
 Fausnaugh M. M., et al., 2017, *ApJ*, 840, 97
 Ferland G. J., & Netzer H., 1983, *ApJ*, 264, 105
 Ge X., Bian W. H., Jiang X. L., Liu W. S., Wang X. F., 2016, *MNRAS*, 462, 966
 Grier C. J., Peterson B. M., Pogge R. W., et al., 2012, *ApJ*, 755, 60
 Grier C. J., Trump J. R., Shen Y. et al., 2017, *ApJ*, 851, 21
 Ho L., 2008, *ARA&A*, 46, 475
 Ho L., Kim M., 2014, *ApJ*, 789, 17
 Jin C., Martin W., Chris D., 2012, *MNRAS*, 425, 907
 Kaspi S., et al., 2005, *ApJ*, 629, 61
 Kaspi S., et al., 2000, *ApJ*, 533, 631
 Kilerci Eser E., Vestergaard M., Peterson B. M., Denney K. D., Bentz M. C., 2015, *ApJ*, 801, 8
 Kokubo M., & Minezaki T., 2019, *MNRAS*, arxiv: 1904.08946
 Kormendy J., Ho L. C., 2013, *ARA&A*, 51, 551
 Li Y. R., et al., 2018, *ApJ*, 869, 137
 Lu K. -X., et al., 2016, *ApJ*, 827, 118
 Lusso E., et al., 2012, *MNRAS*, 425, 623
 Marconi A., et al., 2004, *MNRAS*, 351, 169
 Martínez-Aldama M. L., Czerny B., Kawka D., et al. 2019, preprints (arXiv: 1903.09687)
 McConnell N. J., et al., 2011, *Nature*, 480, 215
 Mejia-Restrepo J. E., et al., 2018, *Nature Astronomy*, 2, 63
 Merloni A., Heinz S., Di Matteo T., 2003, *MNRAS*, 345, 1057
 Pancoast A., et al., 2018, *ApJ*, 856, 108
 Park D., Kelly B. C., Woo J.-H., Treu T. 2012, *ApJS*, 203, 6
 Pei L., et al., 2014, *ApJ*, 795, 38
 Pei L., et al., 2017, *ApJ*, 837, 131
 Peterson B. M., 1993, *PASP*, 105, 247
 Peterson B. M., et al., 2000, *ApJ*, 540, L13
 Peterson B. M., et al., 2004, *ApJ*, 613, 682
 Peterson B. M., et al., 2014, *ApJ*, 795, 149
 Planck Collaboration, et al., 2014, *A&A*, 571, 16
 Shakura N. I., & Sunyaev R. A. 1973, *A&A*, 24, 337
 Shen Y., et al., 2011, *ApJS*, 194, 45
 Shen Y., Ho L. C., 2014, *Nature*, 513, 210
 Shen Y., et al., 2015, *ApJ*, 805, 96
 Shen Y., et al., 2019, *ApJS*, 241, 34
 Sulentic J. W., Marziani P., Dultzin-Hacyan D., 2000, *ARA&A*, 38, 521
 Tremaine S., et al., 2002, *ApJ*, 574, 740
 Trump J. R., et al., 2011, *ApJ*, 733, 60
 Vestergaard M., Peterson B. M., 2006, *ApJ*, 641, 689
 Wang J. M., et al., 2013, *PhRvL*, 110, 081301
 Wang J. M., Du P., Li Y.-R., et al., 2014a, *ApJ*, 792, L13
 Wang J. M., Qiu J., Du P., & Ho L. C., 2014b, *ApJ*, 797, 65
 Wang J. M., Du P., Brotherton M. S., et al. 2017, *NatAs*, 1, 775
 Wang C., Yu L. M., Bian W. H., Zhao B. X., 2019, *MNRAS*, 487, 2463
 Williams P. R., Pancoast A., Treu T., et al., 2018, *ApJ*, 866, 75
 Woo J.-H., et al., 2015, *ApJ*, 801, 38
 Yu L. M., Wang C., Bian W. H., Zhao B. X., 2019, *MNRAS*, 488, 1519
 Yuan F., & Narayan R., 2014, *ARA&A*, 52, 529
 Zhang Z. -X., et al., 2019, *ApJ*, 876, 49

Table 1. The properties of 120 RM AGNs.

Name	τ (days)	$\log L_{5100}$ $\log \text{erg s}^{-1}$	FWHM (km s^{-1})	$\sigma_{\text{H}\beta}$ (km s^{-1})	$D_{\text{H}\beta}$	R_{Fe}	$\log M_{\text{BH},F}$ ($\log M_{\odot}$)	$\log M_{\text{BH},\sigma}$ ($\log M_{\odot}$)	$\log M_{\text{BH},c}$ ($\log M_{\odot}$)	$\log \dot{\mathcal{M}}_F$	$\log \dot{\mathcal{M}}_{\sigma}$	$\log \dot{\mathcal{M}}_c$	Ref
(1)	(2)	(3)	(4)	(5)	(6)	(7)	(8)	(9)	(10)	(11)	(12)	(13)	(14)
SEAMBH													
Mrk335	$8.7^{+1.6}_{-1.9}$	43.69 ± 0.06	2096 ± 170	1470 ± 50	1.43 ± 0.09	...	$6.87^{+0.10}_{-0.13}$	$7.21^{+0.08}_{-0.11}$	$7.33^{+0.10}_{-0.13}$	$0.53^{+0.13}_{-0.13}$	$0.53^{+0.13}_{-0.13}$	$0.53^{+0.13}_{-0.13}$	1, 2, 3*
Mrk335	$16.8^{+4.8}_{-4.2}$	43.76 ± 0.06	1792 ± 3	1380 ± 6	1.30 ± 0.00	...	$7.02^{+0.11}_{-0.12}$	$7.45^{+0.11}_{-0.12}$	$7.55^{+0.11}_{-0.12}$	$0.63^{+0.13}_{-0.13}$	$0.63^{+0.13}_{-0.13}$	$0.63^{+0.13}_{-0.13}$	2, 3, 4*

Note. For a object with multiple measurements, the dimensionless accretion rate $\dot{\mathcal{M}}$ is calculate by the weighted average of the black masses. Names in boldface are the weighted averages of all the measurements. * means that the MCMC black hole mass is used to calculate the dimensionless accretion rate. Reference: 1: Du et al. (2015), 2: Du et al. (2016a), 3: Collin et al. (2006), 4: Bentz et al. (2013), 5: Grier et al. (2012), 6: Bentz et al. (2009a), 7: Du et al. (2018), 8: Du et al. (2016b), 9: Shen et al. (2015), 10: Grier et al. (2017), 11: Shen et al. (2019), 12: Bentz et al. (2009b), 13: Denny et al. (2010), 14: Peterson et al. (2000), 15: Bentz et al. (2006), 16: Fausnaugh et al. (2017) 17: Zhang et al. (2019) 18: Denny et al. (2006) 19: Bentz et al. (2014), 20: Lu et al. (2016), 21: Pei et al. (2017), 22: Barth et al. (2013), 23: Pei et al. (2014), 24: Peterson et al. (2014), 25: Ho & Kim (2014), 26: Barth et al. (2015), 27: Williams et al. (2018), 28: Bentz et al. (2016a), 29: Bentz et al. (2016b)

Table 2. The results of of the multivariate liner regression. The α_1 , α_2 and β_1 is defined by: $y = \alpha_1 x_1 + \alpha_2 x_2 + \beta_1$. The σ_{int} is the intrinsic scatter of this relation. The uncertainties of each value is derived from bootstrap simulation as described in Section 3.2. The last two column are the Spearman correlation coefficient r_s and probability of the null hypothesis p_{null} , we highlighted the correlations with the significant value ($|r_s| > 0.85$) in boldface.

		α_1	α_2	β_1	σ_{int}	r_s	p_{null}
$\log R_{\text{BLR}}(\text{H}\beta) = \alpha_1 \log l_{44} + \alpha_2 \log \dot{\mathcal{M}}_F + \beta$	All Sources	0.45 ± 0.03	-0.10 ± 0.02	1.36 ± 0.02	0.21 ± 0.02	0.803	0.26E-27
	Exclude SDSS-RM	0.52 ± 0.03	-0.14 ± 0.02	1.45 ± 0.02	0.15 ± 0.02	0.919	0.14E-30
$\log R_{\text{BLR}}(\text{H}\beta) = \alpha_1 \log l_{44} + \alpha_2 \log \dot{\mathcal{M}}_{\sigma} + \beta$	All Sources	0.45 ± 0.03	-0.12 ± 0.02	1.33 ± 0.02	0.21 ± 0.02	0.810	0.38E-28
	Exclude SDSS-RM	0.54 ± 0.03	-0.21 ± 0.02	1.42 ± 0.02	0.11 ± 0.02	0.941	0.17E-35
$\log R_{\text{BLR}}(\text{H}\beta) = \alpha_1 \log l_{44} + \alpha_2 \log \dot{\mathcal{M}}_c + \beta$	All Sources	0.60 ± 0.03	-0.31 ± 0.03	1.28 ± 0.02	0.13 ± 0.02	0.883	0.16E-44
	Exclude SDSS-RM	0.62 ± 0.02	-0.31 ± 0.02	1.35 ± 0.02	0.05 ± 0.04	0.952	0.12E-43
$\log R_{\text{BLR}}(\text{H}\beta) = \alpha_1 \log l_{44} + \alpha_2 D_{\text{H}\beta} + \beta$	All Sources	0.39 ± 0.02	0.03 ± 0.04	1.28 ± 0.09	0.24 ± 0.02	0.733	0.18E-20
	Exclude SDSS-RM	0.44 ± 0.03	0.03 ± 0.04	1.33 ± 0.08	0.21 ± 0.02	0.843	0.13E-20
$\log R_{\text{BLR}}(\text{H}\beta) = \alpha_1 \log l_{44} + \alpha_2 R_{\text{Fe}} + \beta$	All Sources	0.42 ± 0.03	-0.28 ± 0.04	1.53 ± 0.08	0.23 ± 0.02	0.739	0.10E-19
	Exclude SDSS-RM	0.48 ± 0.03	-0.38 ± 0.04	1.67 ± 0.09	0.17 ± 0.02	0.876	0.61E-22